Wear 456–457 (2020) 203386

Contents lists available at ScienceDirect

Wear

journal homepage: http://www.elsevier.com/locate/wear

Characteristics of carbide-free medium-carbon bainitic steels in high-stress abrasive wear conditions

Oskari Haiko [a,*], Pentti Kaikkonen [a], Mahesh Somani [a], Kati Valtonen [b], Jukka Kömi [a]

[a] Materials and Mechanical Engineering, Centre for Advanced Steels Research, University of Oulu, Finland
[b] Materials Science and Environmental Engineering, Tampere Wear Center, Tampere University, Finland

ARTICLE INFO

Keywords:
Steel
Bainite
Wear testing
Abrasion
Microstructure

ABSTRACT

This study encompasses a comprehensive account of the abrasive wear properties of carbide-free, ultrahigh-strength bainitic steels processed through ausforming at three different temperatures well below the recrystallization stop temperature followed by bainitic transformation at temperatures close to the M_s temperature. Five medium-carbon, high-silicon compositions were designed for the study by suitably varying the alloying levels of carbon, vanadium, niobium, molybdenum, and aluminum. While ausforming at lower temperatures enabled a large number of nucleation sites leading to significant refinement of bainitic laths, the decomposition of austenite at relatively low transformation temperatures was accelerated due to the presence of a high dislocation density, thus enabling completion of bainitic transformation in a reasonable length of time. The steels were characterized in respect of microstructural features and mechanical properties, besides evaluation of wear resistance through a high-stress abrasive wear testing method with natural granite abrasives. The microstructures comprised different fractions of bainitic ferrite and/or granular bainite (56–68%), martensite (0–25%), besides a significant fraction of retained austenite (20–34%) manifesting as pools and also interlath films, depending on the ausforming conditions and subsequent cooling paths. A tensile strength of 1900 MPa level was achieved with hardness exceeding 500 HV for the medium-temperature ausformed steel containing a high carbon content that also showed lowest mass loss in the wear test. The hardness-to-mass loss ratio appeared highly promising with some of the carbide-free bainitic steels on par with or better than the reference martensitic steel. The high work-hardening capability as a consequence of the strain-induced austenite to martensite transformation was considered as the main factor for the superior abrasive wear resistance of the carbide-free bainitic steels.

1. Introduction

Various grades of high-hardness steels that are categorized according to the surface hardness levels are used in high-stress abrasive conditions. These steels are typically ultrahigh-strength martensitic steels with surface hardness greater than 500 HV. The fabrication of quenched, and often also tempered, martensitic steels is a well-recognized method to produce hard, high-strength materials for various applications. The composition design involves lean, cost-effective alloying including the carbon content that can be adjusted along with the process design to have suitable mechanical properties for different wear systems and environments. Abrasive wear environment usually requires high initial surface hardness to minimize the mass loss of the material. Martensitic steels are therefore preferred as protective materials against abrasion owing to the high strength and hardness of the martensite phase.

Lately many studies have focused on different phases or phase mixtures to understand the effect of microstructure on the wear resistance of steels, including the quenched and partitioned (Q&P) steels, different types of bainitic steels and some other multiphase steels [1–6]. Of these novel concepts, carbide-free bainitic (CFB) steels are believed to be the most studied multiphase steels in the past decade [7–10], though the concept of ultrahigh-strength bainitic steels has been introduced even earlier [11]. It has been shown that wear resistance is not solely dependent on the initial hardness of the steels, but the microstructural features too have a noticeable effect on the wear behavior of steels [12–15]. In other words, the types and fractions of different phases alter the wear properties naturally depending on the wear systems and conditions. However, comparisons have often been made between steels of different microstructures with relatively low hardness levels, when compared to that of the martensitic steels. Undoubtedly, the main

* Corresponding author.
E-mail address: oskari.haiko@oulu.fi (O. Haiko).

https://doi.org/10.1016/j.wear.2020.203386
Received 23 March 2020; Received in revised form 28 May 2020; Accepted 13 June 2020
Available online 14 June 2020

challenge has since been the difficulty of producing ultrahigh-strength steels other than the martensitic steels with hardness exceeding 500 or 600 HV, especially in combination with more robust processing methods that simulate industrial scale production lines.

In fact, an increasing number of studies have emerged recently presenting different types of bainitic steels with high hardness levels that are comparable to the ultrahigh-strength martensitic steels [3,4,16–18]. The latter steels mainly comprise of martensitic matrix with possible presence of some finely distributed retained austenite (< 5%), whereas carbide-free bainitic steels may contain significant amount of austenite, up to 30% or more, retained at room temperature due to significant carbon enrichment. As with other types of multiphase steels, retained austenite could provide better ductility, toughness, and work-hardening capabilities that may be indirectly beneficial in terms of wear resistance. Therefore, novel processing techniques were utilized to produce extremely refined carbide-free bainitic steels with significant fractions of finely divided retained austenite for characterization in respect of abrasive wear properties.

The main objective of this work was to study the mechanical properties, microstructural features and wear performance of five high-silicon, medium carbon bainitic steels, ausformed at three different temperatures: i) just below recrystallization stop temperature, ii) in the bay between ferrite and bainite C-curves and iii) below the bainite start temperature. Phase transformation temperatures and C-curves for similar steels were acquired in previous study published by Kaikkonen et al. [19]. The wear testing was conducted with application-oriented high-stress abrasive testing method. For comparison, a commercial 500 HB grade martensitic steel was included in the wear testing.

2. Materials and methods

The chemical compositions of the five experimental steels in weight percentages are shown in Table 1. Steels A, B, C and D were alloyed with 0.4% carbon, while Steel E contained 0.5% C. All five compositions had 2.0% Mn and 0.7% Cr, in weight percentages. In steel B the Mo content was increased to 0.3% to observe the strengthening effect of molybdenum, whereas in steels C, D, and E, vanadium was used as a strengthener. Manganese is a strong austenite stabilizer and all five compositions were designed to have good austenite stability to enable straining in austenite well below recrystallization stop temperature prior to isothermal holding at the desired bainite transformation temperature. On the other hand, silicon as a strong graphitizer is recognized to prevent carbide precipitation during isothermal holding. For the sake of comparison, in Steel D, a part of the silicon was replaced with aluminium (0.50%), which is also a potent ferrite former and prevents carbide formation during isothermal holding in the bainitic regime. Despite its plausibly harmful effect on the hardness of the steel, aluminium is known to accelerate the bainitic transformation and is considered beneficial in completing the bainite reaction or achieving a high fraction of bainite in a reasonable length of time, thus reducing the amount of untempered, high carbon martensite formed during final cooling to room temperature.

Five compositions were cast in blocks of 150 × 150 × 500 mm, which were then subjected to homogenization annealing at 1250 °C for 24 h, followed by rough rolling down to a thickness of 45 mm (~70% reduction in rough rolling). After the long annealing at such high temperature, some decarburization occurred on the surface and thus, about 2 mm was milled away from both sides of the rough-rolled and homogenized blocks. One block of each composition was processed through one of the three different ausforming processing routes (see Fig. 1) that comprised hot rolling well above recrystallization stop temperature, followed by ausforming planned at either 850 °C (HT), 550 °C (MT) or 450 °C (LT; 420 °C), ending up to a thickness of 12 mm (~70% of total reduction). The experimental ausforming temperatures, however, were ~820, ~550 and ~420 °C, respectively. Hereinafter, the steel will be recognized by its ausforming condition and the steel code, e.g. HT-A, MT-C, etc. Following ausforming, all 12 mm plates were cooled down to 350 °C and held there isothermally for 60 min for facilitating bainite transformation.

Mechanical properties were evaluated in respect of tensile properties as well as Vickers hardness data. Tensile properties were measured using round specimens (ø6 mm × 25 mm gauge length) according to EN 10002-1 standard in a 100 kN Zwick Roell tensile testing device, three tests each for specimens extracted in rolling direction (RD) for all the steels. For Vickers hardness measurements with a Duramin A300 instrument, at least ten indentation measurements were made for each sample using a 10 kgf load.

Metallographic characterization was carried out with a Keyence VK-X200 laser scanning confocal microscope, a Zeiss Sigma field emission scanning electron microscope (FESEM) with 5 kV acceleration voltage and a Rikagu SmartLab X-Ray diffractometer equipped with a Co K_α source at a scanning rate of 7° min^{-1} over the range of $2\theta = 45–130°$. Phase fractions were estimated using both X-Ray diffraction (XRD) as well as image analysis on SEM pictures, more precisely by point counting method according to ASTM E 562 standard [20]. SEM observations for the point calculations were made at 1 mm depth and mid-thickness of the plates, as the temperature during thermomechanical processing was monitored in the core of the plate. The cross-sectional samples were prepared by polishing and etching with 2% Nital prior to the microscopy.

Wear testing was done at Tampere Wear Center, Tampere University, Finland. The selected method was performed on a dry-pot tester, an

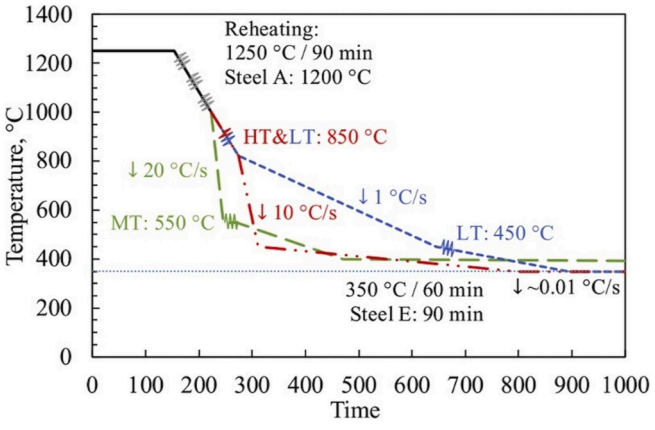

Fig. 1. Schematic sketch of the thermomechanical processing routes.

Table 1
Chemical compositions of the tested steels (wt.%, balance Fe). 500 HB showing the nominal maximum content, from brochure sheet.

Material	C	Si	Mn	Al	Cr	Mo	V	Nb
Steel A	0.40	1.30	2.0	<0.01	0.70	<0.01	0.02	<0.01
Steel B	0.40	1.30	2.0	<0.01	0.70	**0.30**	0.02	**0.02**
Steel C	0.40	1.30	2.0	<0.01	0.70	<0.01	**0.10**	**0.02**
Steel D	0.40	**1.00**	2.0	**0.50**	0.70	<0.01	**0.10**	**0.02**
Steel E	**0.50**	1.30	2.0	<0.01	0.70	<0.01	**0.10**	**0.02**
500 HB	0.30	0.80	1.70	–	1.50	0.50		–

application-oriented pin-mill type tester for high-stress abrasive wear testing. The test procedure has since been extensively used for evaluating the abrasive wear performance of various steels and the imposed test conditions often closely simulated the real-world wear systems, especially existing in mining and mineral handling environments when tested with dry gravel bed [3,21–23]. The test set-up and experimental parameters were very similar to those used in a previous study conducted by Haiko et al. [24] and is briefly outlined here. The device comprises a shaft fitted with the sample holders and a steel pot. Fig. 2a presents a view of the experimental facility. The samples are rotated inside the pot filled with abrasives. The granite from Kuru quarry, Finland, sieved to a size distribution of 8–10 mm was used as the abrasive medium. The shaft inside the pot was rotated at 250 rpm (sample tip speed 2.5 m/s). Four samples were tested at each test period (60 min) and one of the samples was always the reference material (500 HB steel). The total test time (240 min) for each experiment consisted of four 60 min periods. Between the periods, the samples were weighed, the gravel was replenished, and the position of the samples was changed. The gravel batch for each test period consisted of 9000 g of granite. 1350 g of quartzite (100–600 μm, Nilsiä quarry, Finland) was used to prevent the granite from packing underneath the tester shaft head. The sample dimensions were 64 × 40 × 10 mm and the orientation was +45° to normal. Two samples of each CFB material were tested.

The worn materials were inspected after the wear testing. Surface roughness measurements (R_q, root mean square height) based on the ISO 4287-1997 standard [25] were conducted on an area (3.4 × 2.3 mm) marked in Fig. 2b (1) with three measurements per sample. Measurements were done with the laser scanning confocal microscope. The cross-sectional samples for the characterization of the deformed surface were prepared near the most worn part (Fig. 2b, dashed line marked with 2). Back-scatter electron (BSE) images of the surface embedded with granite were taken on the area marked with number 3 in Fig. 2b. The granite area coverage was calculated with the aid of a Fiji image processing tool package based on ImageJ open-source image analysis software. Three images and analysis were done on each sample.

In order to prepare a geometrical magnification of the tribolayers, the tapered samples of the wear surfaces were prepared in a similar way as presented by Valtonen et al. [21]. The samples were cut near the area marked with number 3 in Fig. 2b. Samples were then placed on 10° angle to horizontal using a taper section sample holder, cold-mounted, and further polished and etched for microscope inspection and microhardness measurements. Microhardness measurements were conducted on the tapered samples as close to the interface as possible, between the granite covered surface and the deformed material underneath. Measurements were made on three different spots with a minimum of five indentations. The used tester was CSM Instruments MHT-Z-AE and the indentations were made with 0.25 N force.

3. Results

3.1. Microstructures of the studied steels

Thermomechanically controlled processing according to Fig. 1 resulted in various microstructures comprising different phase mixtures depending on the deformation parameters (temperature, strain, and strain rate) as well as the thermal paths the steels were subjected to. Fig. 3 presents representative FESEM micrographs recorded on various samples, revealing varying mixtures of bainitic ferrite, granular bainite, (untempered, high-carbon) martensite and retained austenite. Phase fractions and the average size of bainitic ferrite features (BFF) based on the image analysis as well as the phase fractions estimated through XRD measurements are presented in Table 2. As regards BFF, all kind of bainitic features were considered in the measurements, including the thickness of bainite laths and plates as well as the diameter of granular bainite, which explains the scatter in the data and relatively high coarseness of the bainite compared to values reported in literature [26,27].

The samples, following MT ausforming at about 500 °C, were cooled relatively slowly because of the difficulties in accurately controlling the temperature down to the isothermal holding temperature of 350 °C. Hence, the fraction of bainite transformation was relatively low owing to the higher transformation temperature, as most of the 1 h holding time (practically, non-isothermal) was spent during cooling to 350 °C itself (see Fig. 1). Steel E with 0.5% C and microalloy additions of Nb and V, should presumably have still further delayed transformation, which was incomplete during holding for 1 h after MT ausforming at 500 °C, leading to the transformation of a high fraction of untransformed austenite into martensite during final cooling.

All steels contained significant fraction (20.0–33.6%) of retained austenite, either as coarse (5–10 μm) pools or fine, inter-lath films, as fine as 30–50 nm in thickness. However, it was seen that thin austenite films could be observed also in the microstructures where bainite plates were coarse, while the size of the retained austenite mainly correlated linearly with BFF. The commercial 500 HB steel was only studied with FESEM and confirmed fully martensitic. Previous measurements [1] for the 500 HB steel had shown that no retained austenite or only very low fraction of austenite could be observed with XRD.

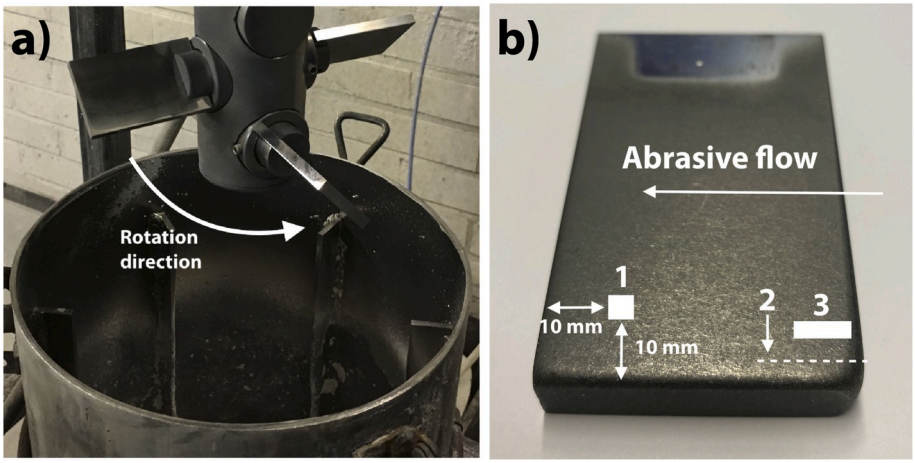

Fig. 2. a) Dry-pot tester fitted with four samples at +45° angle to normal and b) worn sample marked with measured and investigated areas (not in true scale): 1. surface roughness, 2. cross-sectional samples for microscopy (laser and FESEM), and 3. FESEM (BSE) imaging and taper sectioning area.

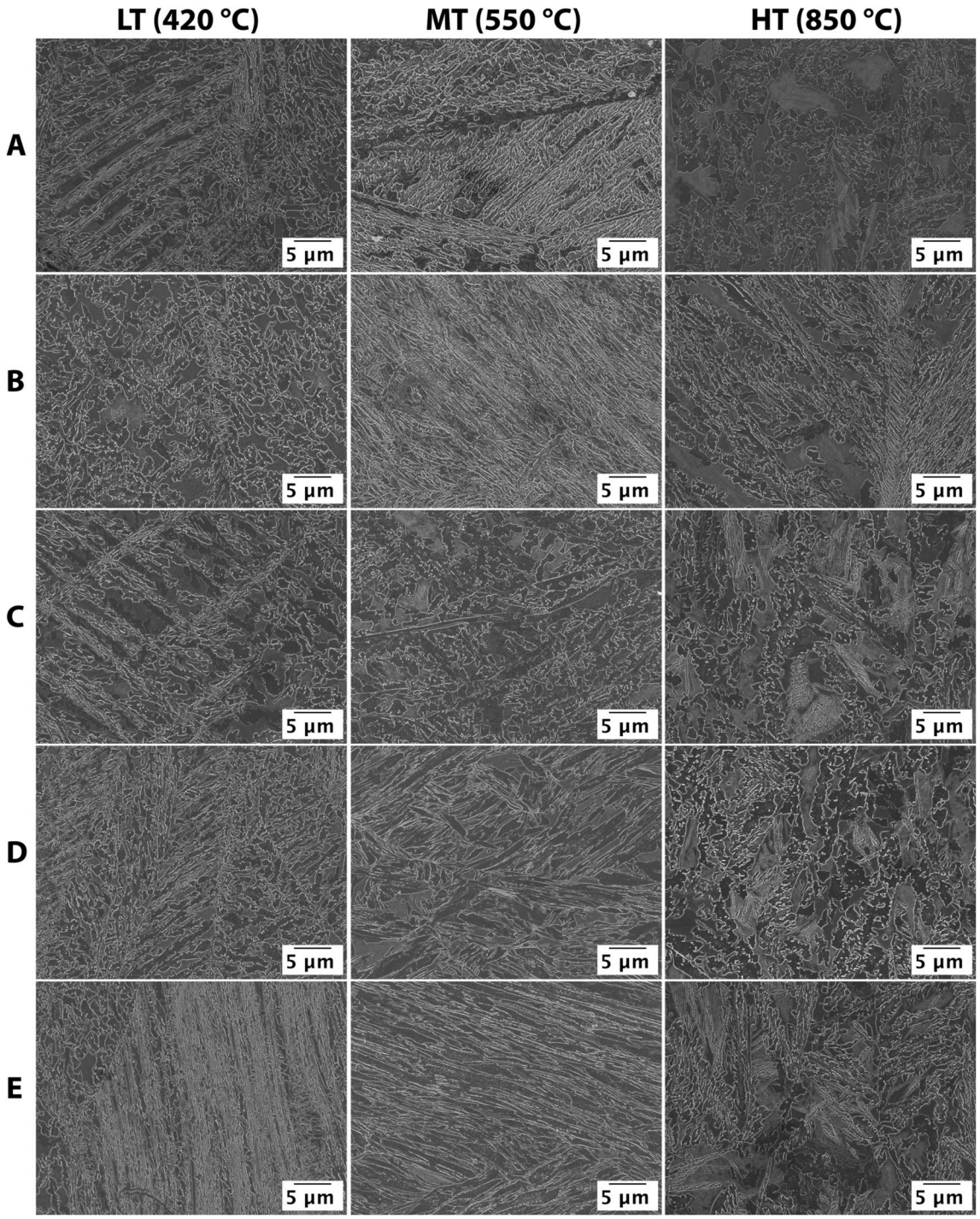

Fig. 3. Microstructures of the tested steels; images taken at 1 mm depth below surface at rolling-to-normal direction.

3.2. Mechanical properties

The mechanical properties for the tested bainitic steels are given in Table 3. The results include tensile properties (0.2% offset yield strength ($R_{p0.2}$), ultimate tensile strength (R_m), and uniform elongation (A_g)) measured at room temperature, and the bulk hardness (HV10). The retained austenite fractions stabilized down to room temperature and BFF are also included in Table 3 for ready comparison. With significant fractions of fine austenite retained at room temperature, low values of yield ratio were not surprising. The highest hardness (535 ± 22 HV10) of the sample MT-E corroborates its high tensile strength (1912 ± 9 MPa) to relatively higher carbon content in the steel (0.5% C), besides a significant fraction of both fine bainite (63%; 368 ± 24 nm) and martensite (16%) together, and consequently a slightly reduced fraction of austenite (22.9%) in the microstructure than seen in HT-E (27.7%) and LT-E (33.6%) samples, respectively. Similarly, HT-E sample displayed higher hardness (472 ± 17 HV10) and tensile strength (1469 ± 24 MPa) compared to LT-E sample (445 ± 10 HV10 and 1462 ± 20 MPa), owing to the finest bainite (175 ± 15 nm) measured, besides a lower fraction of retained austenite. Interestingly, the difference in strength between HT-E and LT-E was considered minor, even though LT-E with a higher fraction of retained austenite showed considerably higher uniform elongation (25.2 ± 0.5%), because of the enhanced stability of the retained austenite, which influenced its higher strain-

Table 2
Phase fractions of experimental steels.

Material	Image Analysis			XRD
	Bainitic ferrite [%]	Martensite [%]	BFF [nm]	Retained austenite [%]
LT-A	61	4	343 ± 43	29.0
LT-B	56	0	686 ± 39	29.8
LT-C	56	14	532 ± 41	29.8
LT-D	62	0	444 ± 17	26.5
LT-E	61	0	395 ± 35	33.6
MT-A	50	25	285 ± 15	21.3
MT-B	67	4	329 ± 18	20.0
MT-C	59	12	574 ± 33	20.8
MT-D	52	21	400 ± 34	22.6
MT-E	63	16	368 ± 24	22.9
HT-A	60	21	523 ± 37	20.8
HT-B	58	22	532 ± 28	22.9
HT-C	60	22	371 ± 30	23.6
HT-D	58	22	352 ± 27	24.0
HT-E	68	3	175 ± 15	27.7

hardening ability, thus contributing to both elongation as well as tensile strength. Nevertheless, the morphology of the bainite could be described as thin, lath-like sheaves in LT-E sample, whereas in HT-E sample, the shape was more granular and these are the main contributors to the strength depending on their respective fractions, i.e. 61 % and 68% in the steels LT-E and HT-E, respectively.

However, the highest hardness for most compositions (except for Steel D) was obtained in MT-ausformed condition, due to somewhat lower fractions of austenite and higher fractions of martensite in some cases. Moreover, the lowest hardness for each composition was obtained in LT steels, probably originated from slower cooling from 850 °C to 450 °C and relatively lower deformation at the ausforming temperature compared to HT and MT ausforming conditions.

Referring to Table 2, sample LT of steel A (LT-A), showed significant fraction of retained austenite (29%) following 1 h holding at 350 °C suggesting extensive bainite formation (61%) during isothermal holding and hence, only little martensite formation (4%) during final cooling, resulting in somewhat lower hardness (below 400 HV10) than other LT samples, Table 3. Unexpectedly, the second highest tensile strength (1702 ± 65 MPa) was displayed by steel MT-A, not only because of the high martensite fraction (25%), but also due to fineness of the bainitic structure (285 ± 15 nm). For instance, MT-D had approximately similar phase fractions as MT-A, but remarkably coarser bainite decreased its hardness (418 ± 19 HV10) and ultimate tensile strength (1500 ± 7 MPA) to comparatively lower level. In general, the mechanical properties of the tested bainitic steels were high and in terms of ultimate tensile strength, MT steels were comparable to commercial ultra-high strength martensitic steels. Yield strengths, however, were considerably lower than in martensitic steels obviously as a consequence of lower strength of bainite, but the strain hardening capability of the tested bainitic steels, in general, was far superior to the commercial steels.

3.3. Wear test results

3.3.1. Mass loss

The wear test results in respect of mass loss following the dry-pot testing are presented in Table 4. The results are also plotted on a chart in Fig. 4a. Most of the CFB steels showed abrasive wear performance correlating with the initial hardness, but some exceptions to this established phenomenon did also exist. Unsurprisingly, the lowest mass loss was measured for the sample with the highest initial hardness (MT-E; 535 ± 22 HV10) obviously as a result of higher carbon level (0.5% C) in the steel besides combined high fraction of martensite and bainitic ferrite, whereas the sample LT-A with the lowest initial hardness (375 ± 7 HV10) showed the highest mass loss.

The most interesting steel sample, however, was the LT-C which had very good hardness-to-mass loss ratio, i.e. the mass loss was relatively low despite the low initial hardness. Moreover, the BFF of the LT-C was above average (532 ± 41 nm), while retained austenite content was quite high. Also, the MT-E performed very well, but as a consequence of the highest initial hardness. However, the hardness of MT-E was on par with the commercial 500 HB steel while the measured mass loss was lower for the CFB steel.

Table 3
Mechanical properties with standard deviations and retained austenite content of the tested steels.

Material	$R_{p0.2}$ [MPa]	R_m [MPa]	Yield ratio	A_g [%]	Hardness HV10 [kgf/mm^2]	Retained austenite [%]	BFF [nm]
LT-A	807 ± 21	1342 ± 17	0.60	19.8 ± 1.1	375 ± 7	29.0	343 ± 43
LT-B	819 ± 28	1391 ± 24	0.59	18.4 ± 0.5	416 ± 13	29.8	686 ± 39
LT-C	781 ± 18	1413 ± 18	0.55	18.8 ± 0.3	412 ± 7	29.8	532 ± 41
LT-D	833 ± 7	1294 ± 3	0.64	18.2 ± 0.3	393 ± 11	26.5	444 ± 17
LT-E	910 ± 9	1462 ± 20	0.62	25.2 ± 0.5	445 ± 10	33.6	395 ± 35
MT-A	796 ± 62	1702 ± 65	0.47	9.6 ± 1.0	458 ± 18	21.3	285 ± 15
MT-B	870 ± 49	1566 ± 9	0.56	11.0 ± 0.2	455 ± 18	20.0	329 ± 18
MT-C	758 ± 26	1626 ± 32	0.47	11.3 ± 1.2	460 ± 12	20.8	574 ± 33
MT-D	712 ± 20	1500 ± 7	0.47	11.5 ± 0.3	418 ± 19	22.6	400 ± 34
MT-E	821 ± 10	1912 ± 9	0.43	7.9 ± 0.6	535 ± 22	22.9	368 ± 24
HT-A	828 ± 138	1490 ± 2	0.56	10.6 ± 0.2	436 ± 19	20.8	523 ± 37
HT-B	855 ± 6	1423 ± 23	0.60	12.3 ± 0.4	451 ± 13	22.9	532 ± 28
HT-C	713 ± 35	1436 ± 14	0.50	12.3 ± 0.1	435 ± 18	23.6	371 ± 30
HT-D	914 ± 67	1425 ± 14	0.64	11.4 ± 1.2	436 ± 12	24.0	352 ± 27
HT-E	935 ± 39	1469 ± 24	0.64	14.1 ± 0.7	472 ± 17	27.7	175 ± 15
500 HB	1300[a]	1600[a]		–	535 ± 16	–	

[a] Information from manufacturer's data sheet (typical properties).

Table 4
Tested materials with the initial hardness, dry-pot test results (mass loss) and difference to the reference material (500 HB). Standard deviations included.

Material	Hardness HV10 [kgf/mm^2]	Mass loss [g]	Diff. to 500 HB [%]
LT-A[a]	375 ± 7	1.773 ± 0.051	+13.7
LT-B	416 ± 13	1.665 ± 0.016	+6.7
LT-C[a]	412 ± 7	1.547 ± 0.015	−0.8
LT-D[a]	393 ± 11	1.653 ± 0.018	+6.0
LT-E	445 ± 10	1.588 ± 0.027	+1.8
MT-A	458 ± 18	1.583 ± 0.011	+1.4
MT-B	455 ± 18	1.616 ± 0.054	+3.6
MT-C[a]	460 ± 12	1.591 ± 0.026	+2.0
MT-D	418 ± 19	1.653 ± 0.042	+5.9
MT-E[a]	535 ± 22	1.470 ± 0.040	−5.8
HT-A	436 ± 19	1.605 ± 0.019	+2.9
HT-B	451 ± 13	1.572 ± 0.016	+6.7
HT-C[a]	435 ± 18	1.660 ± 0.015	+6.4
HT-D	436 ± 12	1.631 ± 0.081	+4.6
HT-E[a]	472 ± 17	1.560 ± 0.018	+0.0
500 HB[a]	535 ± 16	1.560 ± 0.044	–

[a] Samples selected for further investigation.

In Fig. 4a, the steels have been plotted on hardness vs mass loss chart for better illustration of the differences between the steels in terms of wear resistance. Starting with the LT-ausformed steels, except for the LT-C sample, the other LT samples from steels B and D showed relatively high mass loss, although the hardness of these samples was somewhat low (416 ± 13 and 393 ± 11 HV10, respectively) compared to samples from HT- and MT-ausformed steels. This was essentially because of the relatively high retained austenite contents and little or insignificant martensite formation during final cooling. As mentioned, the LT-A had the highest mass loss, presumably due to the lowest initial hardness together with low fraction of martensite.

At the same initial hardness level of approximately 440 HV10, the wear behavior of the three HT-ausformed steels A, C and D suggested that steel A had the best abrasive wear resistance among the three. This may be correlated to its microstructure, as its austenite content was lower and more interestingly, the BFF was higher than seen in HT-C and HT-D samples. On the other hand, the HT-B with 0.4% C and 451 HV10 hardness showed comparable wear resistance with that of HT-E with 0.5% C and marginally higher hardness of 472 HV10. Initially, the results can be corroborated in respect of microstructures and tensile properties, which show that higher carbon content in HT-E stabilized more austenite to be retained at room temperature after isothermal holding, whereas in HT-B sample, more martensite was formed during cooling to room temperature and explains the role of deformation at high temperature in the no-recrystallization regime (T_{NR} regime), followed by isothermal holding at 350 °C. Nonetheless, there were practically no marked difference in microstructures of HT-A and HT-B samples; HT-B sample had slightly higher retained austenite content (22.9%), but it exhibited better performance in respect of abrasive wear resistance. Presumably, solid solution strengthening with Mo may have caused the difference. The wear behaviour of MT-ausformed samples (steels A, C and B) is not easy to understand because of slow cooling, but the mass loss seems to be marginally higher than the HT-ausformed samples, in general.

Eight wear-tested steel samples were selected for further detailed inspection and study in respect of differences in wear behavior. The selected wear-tested steel samples from Fig. 4a are shown again in Fig. 4b. The LT-C, HT-E, and MT-E were selected due to the low mass loss compared to that of the reference 500 HB steel, despite their widely varying hardness values (412 ± 7, 472 ± 17, and 535 ± 22 HV10, respectively). The other two variants of Steel C (HT-C and MT-C) were also included to study the effect of the processing on the wear performance. The LT-D and LT-A samples were also chosen to represent the steel types with LT-ausforming conditions that resulted in low hardness as well as relatively poor abrasive wear resistance. Also, the reference steel 500 HB was included for comparison. The wear behavior of these eight steel samples including corroboration with the microstructures and properties will be discussed further in the following chapters.

3.3.2. *Surface roughness and granite embedment*

The surfaces of the steel samples were heavily deformed by the hard abrasive particle flow, and also granite particles had embedded on the surface of the samples during testing. Therefore, the surface roughness and granite embedment of the worn steel samples were carefully measured. Previous studies by Haiko et al. [1,24] have shown that both the surface roughness and granite embedment have some correlation with the wear performance, i.e. the lower the mass loss is, the lower the R-values and granite area coverage are. Also, an increase in the initial hardness of the samples seemed to result in smoother surface and less granite embedment of the wear-tested samples. The correlation has been found to be distinctly profound when tested in impact-abrasive conditions with an impeller-tumbler compared to the presently employed abrasive dry-pot method [24].

The surface roughness values are plotted in Fig. 5. There was no clear correlation between the R_q and the mass loss. Though, the MT-E sample with the highest initial surface hardness and the lowest mass loss expectedly did have the smoothest surface after wear testing, but the differences between all the samples were quite minor.

The area covered by granite embedment had slightly better

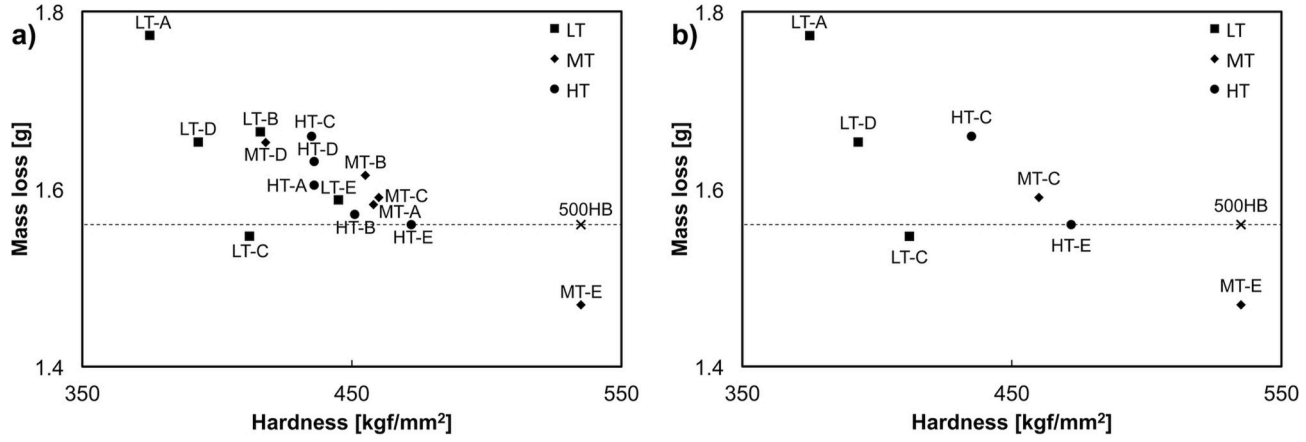

Fig. 4. a) Initial hardness vs mass loss for all tested steels, b) initial hardness vs mass loss for steels that were selected for the detailed characterization. Dashed line shows the 500 HB mass loss.

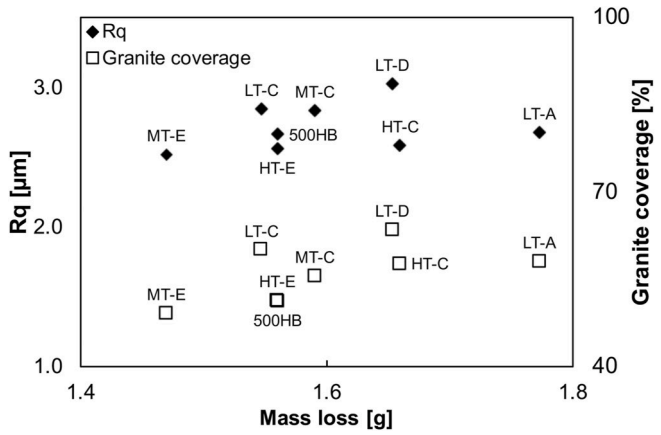

Fig. 5. Surface roughness (R_q) of the worn samples and average area covered by granite.

correlation with the mass loss (Fig. 5). Some examples of the BSE-images are given in Fig. 6. Interestingly, the LT-A sample with the highest mass loss appeared to have less granite embedment and rather smoother surface than some other variants despite having the lowest initial hardness (Figs. 5 and 6a). This could be and indication that the wear mechanisms for the lowest hardness sample has been slightly different from the other samples. The HT-E and 500 HB steels had almost identical area coverage for granite embedment albeit a difference of about 60 HV10 in the initial hardness. Standard deviation for the surface roughness and granite embedment measurements was less than 5%.

3.3.3. *Wear surfaces*

Fig. 7 shows the panorama images of the wear surface cross-sections taken with the laser scanning confocal microscope that provide some general information about the depth of deformation and granite particle penetration. The different microstructural features can also be seen in the images. The most worn sample (LT-A) showed quite a large amount of embedded granite near the surface (Fig. 7a), and the particles appeared to have formed a distinctive tribolayer on the surface, i.e. a mixture of granite and steel. The maximum depth of the deformed microstructure reached approximately 20–25 µm below the surface: the depth of the deformed microstructure was measured from the cross-sectional views by image analysis. Sample LT-C (Fig. 7b) also showed large areas covered by embedded granite, but the thickness of the tribolayer appeared significantly lower in comparison with that of the LT-A sample. The depth of deformation was difficult to measure for the LT-C sample because of the highly orientated features in the microstructure, but an estimated maximum depth was around 17 µm. Similar difficulties were encountered with the LT-D sample (Fig. 7c) when trying to evaluate the deformed microstructure, but it was concluded that the plastic deformation layer had somewhat reached similar depth level as with the LT-C sample (Fig. 7b).

The MT-treated steels MT-C and MT-E (Fig. 7d–e) had some granite embedded, but the deformation depth was slightly lower compared to the LT-steel samples presumably because of the higher initial hardness of the MT-samples, owing to a significant fraction of martensite in these samples, as discussed earlier. The MT-E, sample with the lowest mass loss, showed some shallow pits and particles embedded (Fig. 7e), but the surface, in general, had less damaged appearance compared to the previous samples discussed above. The HT-C sample (Fig. 7f) had a significant amount of abrasives carved into the surface, even though the deformation depth did not exceed 20 µm. A large abrasive particle can be seen embedded to the HT-E sample surface in Fig. 7g, but the given steel showed quite less damage, i.e. only very thin tribolayer was formed and only a low amount of plastic deformation had occurred. This can be attributed to its high hardness (472 HV10) owing to 0.5% C in the steel, though the retained austenite fraction was somewhat high 27.7% compared to other HT-ausformed steels. The commercial 500 HB wear resistant steel (Fig. 7h) had lower amount of plastic deformation compared to the CFB samples. Based on the laser-optical cross-sections, the HT-E and 500 HB samples (Fig. 7g and h, respectively) had the least deformed surfaces, while the lower hardness samples had more abrasive penetration and plastic deformation reached deeper into the bulk material.

The tapered samples are presented in Fig. 8. The images show the transition from the granite covered surface to the deformed material just below the surface (in sub-surface region), i.e. the examination is conducted directly from below the surface, and not from the side like in the case of the cross-sectional samples. As the samples have been prepared at 10° angle, the depth of the visible area changes when moving from top to bottom in the image. Therefore, the 20 µm scale bar (Fig. 8h) corresponds to horizontal direction; the same 20 µm movement in the vertical

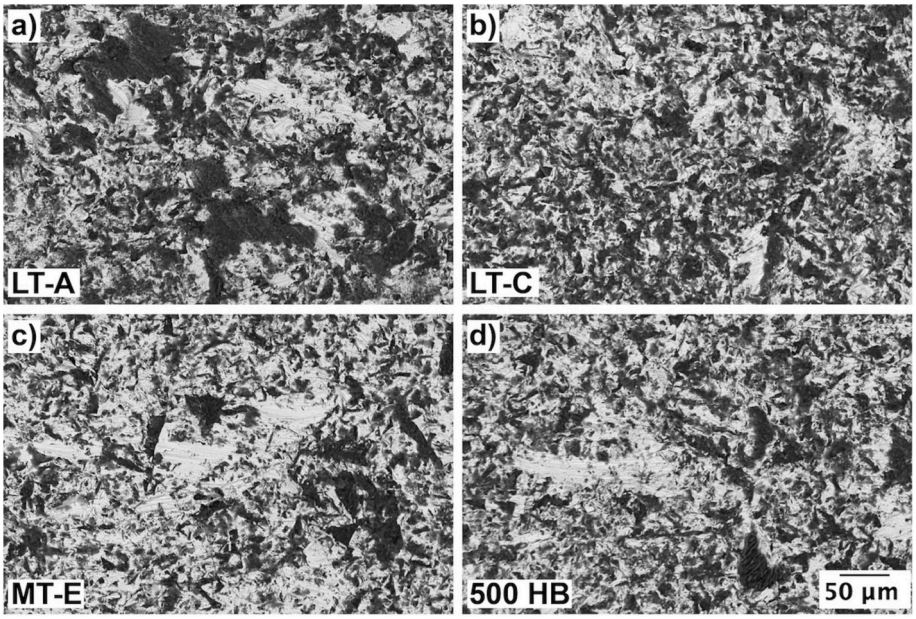

Fig. 6. FESEM BSE images of the wear surfaces: a) LT-A, b) LT-C, c) MT-E, and d) 500 HB.

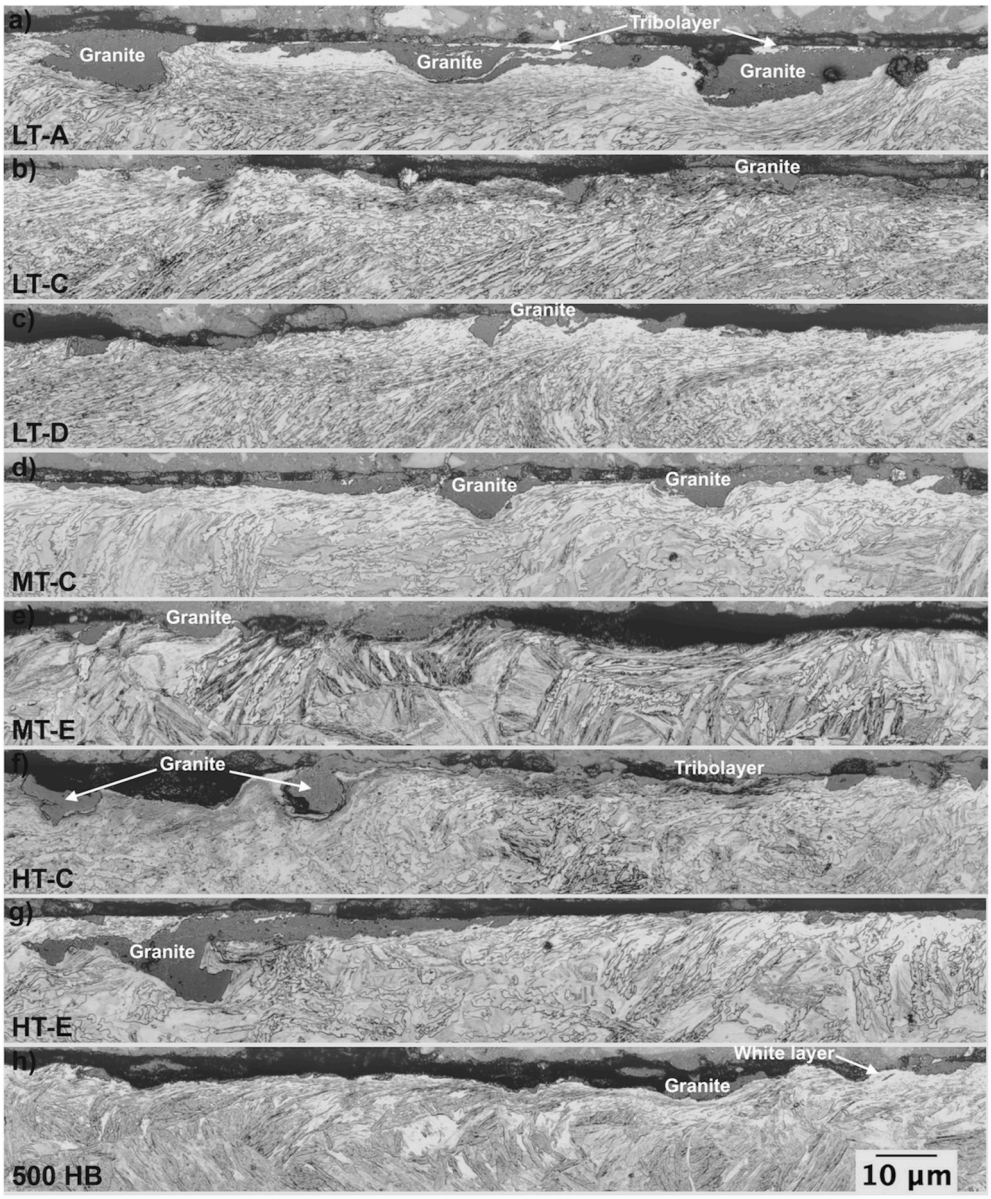

Fig. 7. Laser-optical images of the wear surfaces (cross-sections): a) LT-A, b) LT-C, c) LT-D, d) MT-C, e) MT-E, f) HT-C, g) HT-E, and h) 500 HB. Abrasive flow during the test was from left to right. Dark areas are air gaps between the plastic mount and the sample surface.

direction corresponds approximately 3.5 μm distance (depth). The method enables wider view to the wear surface and the tribolayer. The LT-A sample (Fig. 8a) with the highest mass loss had substantial amount of granite particles attached to the surface, as also noticed from the cross-section samples (see Fig. 7a). The interface between the granite covered surface (top of the image) and the steel bulk beneath the surface extended deeper into the material compared to the other steel samples. The LT-C sample (Fig. 8b) had less damage on the surface, or in other words, the damage did not reach as far beneath the surface as with the LT-A sample. Instead, some large abrasives had attached to the surface, but the number of particles seemed lower than those attached with the LT-A sample. The tapered samples LT-D and MT-C (Fig. 8c and d, respectively) had quite similar appearance, whereas the MT-E sample (Fig. 8e) had large dents and scratches on the surface. The HT-C and HT-E samples (Fig. 8f and g, respectively) had similarities to the LT-D and MT-C samples (Fig. 8c and d, respectively), and no distinctly different features could be stated. The most significant features were found with the 500 HB reference steel sample that had notable amount of white layer formation (Fig. 8h). The fully martensitic structures are more prone to the formation of white layer and shear bands [28], but the clear contrast between the light areas and the bulk material revealed the severely strained and possibly transformed areas, too. It was relatively difficult to observe these features in the already whitish appearing of the CFB samples, presumably because the bainitic steels did exhibit little or no white layer formation or adiabatic shear bands at all.

The FESEM images (Figs. 9–11) show more clearly the detailed surface layer deformation. The severity of the plastic deformation is most visible in the lowest hardness sample LT-A (Fig. 9). The microstructure appeared highly compressed and elongated beneath the granite layer. Similar deformed structures could be observed in other samples as well, but with lesser degree of deformation. The LT-C sample with relatively low initial hardness (412 ± 7 HV10) also showed strong plastic deformation near the surface (Fig. 10a–b). However, the LT-C sample showed some near-nanoscale features closest to the granite embedment near surface (Fig. 10b, closely above the arrow). It could not be ascertained clearly whether this was the white layer or sub-surface shear band structure seen in the confocal microscopy. The formation of a high-hardness layer could be a result of improved work-hardening

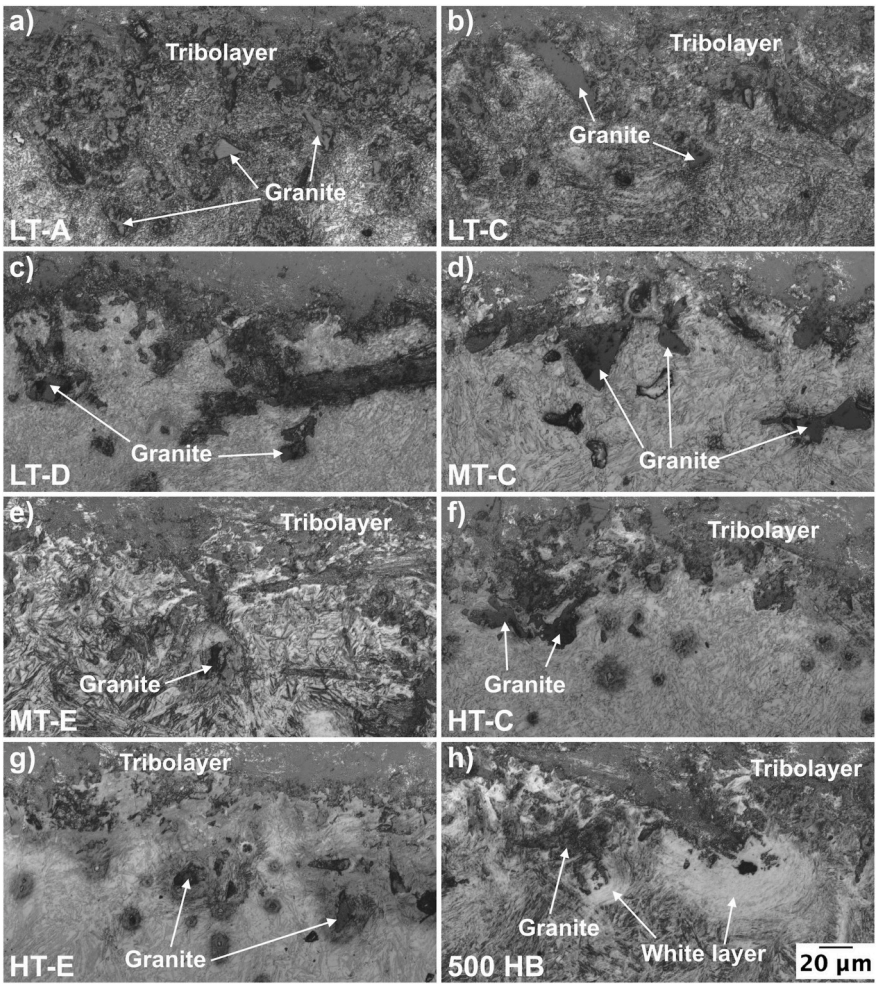

Fig. 8. Laser-optical images of the wear surfaces (tapered samples): a) LT-A, b) LT-C, c) LT-D, d) MT-C, e) MT-E, f) HT-C, g) HT-E, and h) 500 HB.

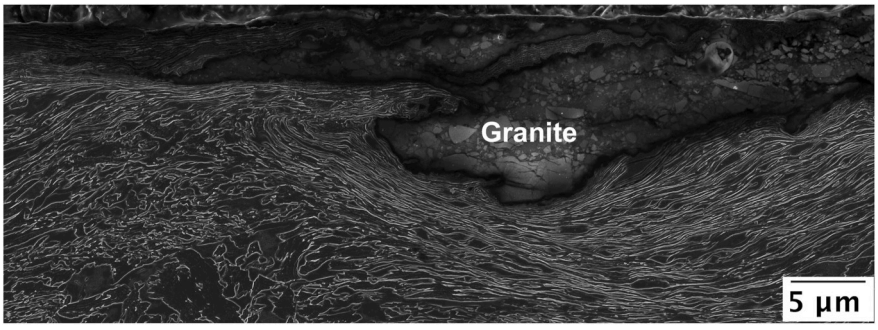

Fig. 9. FESEM image of wear surface (LT-A).

that eventually led to the increased wear performance. Fig. 10 shows the FESEM images of the two samples with the highest initial hardness (MT-E and 500 HB). Both had some white layer formed near the surface as also seen in the confocal microscopy, and is also expected due to the presence of the hard martensite phase.

3.3.4. *Deformed hardness and retained austenite*

Microhardness measurements of the wear surfaces are summarized in Table 5. The deviation for the wear surface hardness data was high due to the highly localized plastic deformation. Nevertheless, a substantial increase in hardness was observed for all the samples. Although the microhardness measurements tend to show somewhat higher hardness compared to the bulk macrohardness testing with higher force [29] (10 kgf here), the comparison between the tested steels revealed that the LT-C and MT-E steels had greater hardness increase compared to the other steels, Table 5. The most interesting observation was made on plotting the mass loss against the wear surface hardness (Fig. 12): the surface hardness of the deformed surface and mass loss of the CFB steel samples nearly resulted in a linear correlation with a high degree of fit, i.e. $R^2 = 0.913$. In other words, the significant increase in hardness of the LT-C sample (about 339 kgf/mm^2 difference) most probably resulted in the relatively good wear performance despite the lower initial hardness. It has been noted earlier that the wear surface hardness correlates better with the wear resistance [30], and now the current results show that

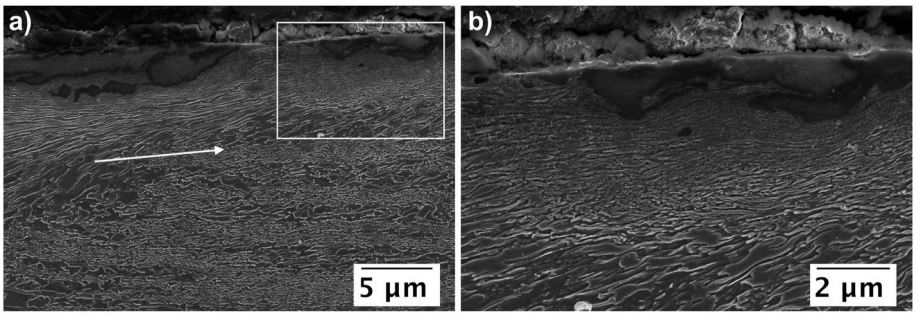

Fig. 10. FESEM images of wear surface (LT-C) with close-up on the right. Arrow indicates the direction of the deformed microstructure and flow direction of the abrasives.

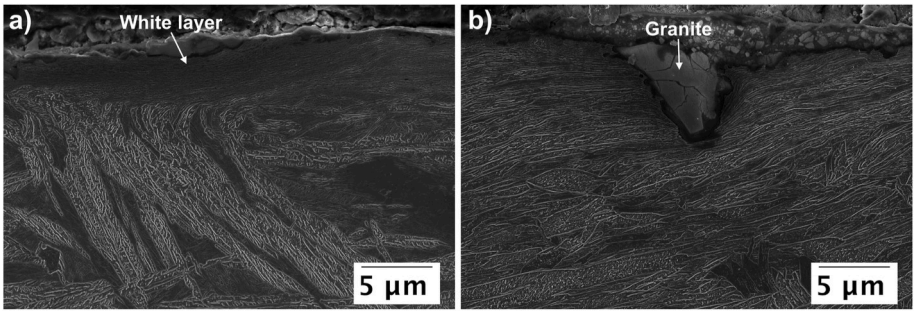

Fig. 11. FESEM images of wear surfaces: a) MT-E and b) 500 HB.

Table 5
Bulk hardness prior to wear testing, surface hardness after testing and retained austenite prior and after wear testing measured with XRD. Bulk hardness was measured with 10 kgf force (HV10, 98.07 N) and deformed hardness with 0.25 N load (Vickers diamond intender).

Material	Bulk hardness [kgf/mm^2]	Deformed hardness [kgf/mm^2]	Difference [kgf/mm^2]	Retained austenite – prior [%]	Retained austenite – after [%]
LT-A	375 ± 7	629 ± 38	254	29.0	6.5
LT-C	412 ± 7	751 ± 79	339	29.8	5.2
LT-D	393 ± 11	671 ± 63	278	26.5	5.4
MT-C	460 ± 12	716 ± 50	256	20.8	2.9
MT-E	535 ± 22	839 ± 64	304	22.9	3.9
HT-C	435 ± 18	708 ± 62	273	23.6	4.1
HT-E	472 ± 17	743 ± 46	271	27.7	11.7
500 HB	535 ± 16	804 ± 83	269	–	–

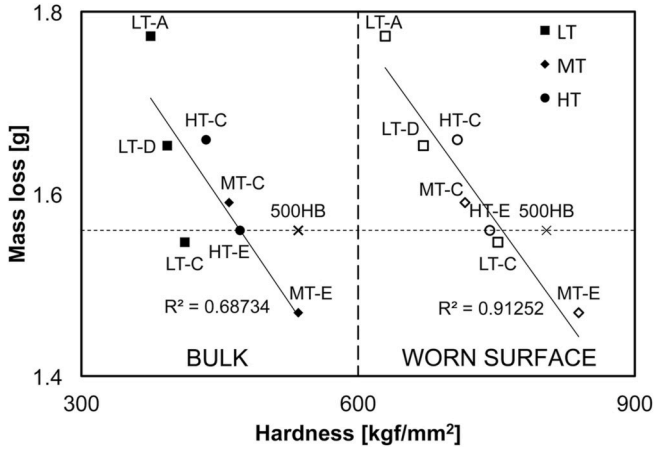

Fig. 12. Initial bulk hardness and deformed surface hardness with mass loss of selected samples (500HB not included in the fitting curve).

effect with the tested CFB steels, as well.

The retained austenite measurements were made on the wear surfaces following the wear tests using the XRD and the results are included in Table 5. It can be seen that all the CFB samples, irrespective of steel type, had some austenite retained even after the testing, but a significant fraction of the austenite had transformed during the abrasive wear testing. The strain-induced transformation of austenite to high-hardness martensite presumably explains the high degree of work-hardening and the increased hardness levels at the surface of the worn steel samples.

4. Discussion

The experimental carbide-free bainitic steels showed some interesting results regarding the mechanical properties and wear performance. The three ausforming methods provided different mechanical properties due to the varying phase content and differences in the bainitic ferrite features. The amount of bainite was generally between 50 to 70%, while the amount of martensite and retained austenite varied as well. The effect of different phase fractions on the mechanical properties was eventually not as clear as expected. The highest initial hardness and tensile strength were measured for the MT-E specimen (535 ± 22 HV10, 1912 ± 9 MPa), but the steel did not exhibit the highest martensite (16%) content nor it showed the least amount of retained austenite (22.9%). The size of bainitic ferrite features (BFF) was somewhat average with (368 ± 24 nm). However, the elongation (7.9 ± 0.6%) was the lowest of all samples, which might indicate that martensite content could have been higher than observed. Nevertheless, the strength levels and hardness of the MT-E were highly promising for a bainitic-martensitic steel. All the other MT-ausformed steels also exhibited higher tensile strength and slightly higher hardness compared to the LT

and HT-samples, while elongation was generally reduced. The BFF values were somewhat inconclusive, but this also applied to the other ausforming methods.

Surprisingly, HT-A represented relatively low retained austenite content (20.8%, second lowest of all studied steels) and coarse BFF (523 ± 37 nm), but it had somewhat higher tensile strength than HT-C and HT-D samples. However, it is interesting to point out that despite the refinement of bainitic structure in C and D samples through the additions of Nb (0.02%) and V (0.1%), the properties were not affected in a positive manner. The HT-ausforming in general resulted in lower tensile strength, but higher yield strength compared to that in the case of LT-ausforming. The mechanical properties of the HT-samples were in between the LT and MT-samples. The lowest ausforming temperature (LT) resulted in a mixture of bainitic ferrite and retained austenite without the presence of a significant amount of martensite. Therefore, the steels produced via LT-ausforming route obviously had the lowest tensile strength and hardness among the three ausforming methods applied, apart from the elongation.

The bainitic steels seemed to show almost linear correlation with the mass loss and initial hardness (see Fig. 4a), with few exceptions. This well-known phenomenon has been seen in multiple studies regardless of the used wear testing device. In the current tests, the initial hardness did have a marked effect on the abrasive wear resistance, but more prominent outcome was the drastic effect of the work-hardened surface on the wear performance. The major work-hardening capability of the CFB steels resulted in some CFB variants to outperform the martensitic steel when comparing hardness to mass loss ratio (LT-C and HT-E) and also in terms of absolute mass loss (MT-E), see Fig. 12. Though, the martensitic 500 HB sample also experienced strong work hardening, it cannot be attributed to the strain-induced transformation of retained austenite to martensite, in the absence of any austenite in the steel. The martensitic steels work-harden during abrasion [21,24], but this often leads to the formation of adiabatic shear bands and white layer, also seen in the current work. These, in turn, might act as sites for easy crack initiation and propagation. However, the amount of white etching layer was low or even absent for the CFB steels. Those CFB samples with more martensite present did show shear bands and white layer formation, but this was still much more suppressed compared to the martensitic steel. The lack of white layer and shear bands could be one possible reason for the lower mass loss compared to the martensitic steel, especially for the lower hardness sample LT-C. However, the LT-C also showed some martensite present in the microstructure based on the image analysis, which in turn might have been beneficial against abrasive wear. Based on the microhardness and XRD measurements of the wear surface, it is quite clear that substantially high work-hardening capability can be attributed for the outstanding wear performance when considering the hardness-to-mass loss ratio.

Among the tested CFB steels and ausforming methods, the results were somehow scattered and no general suggestion on the recommendable ausforming method or composition could be made. The higher carbon composition E was the best composition on average, presumably due to the higher carbon content and therefore due to the increased average hardness. The composition C was included in the further inspection with all the three ausforming methods represented. The lowest mass loss of the composition C samples was measured for the LT-C with the lowest initial hardness, but which had the highest deformed hardness after wear testing. The bainitic ferrite fraction was estimated very close to each other, but the LT-C steel had the most retained austenite present, and the highest fraction of stable inter-lath austenite films instead of blocky austenite, despite mean BFF was the lowest in HT-C. With all the three C-steels almost all retained austenite had transformed during the abrasive wear. Similar to the other CFB steels, the ranking from best to worst in terms of wear performance was dependent on the deformed hardness irrespective of the initial hardness.

Referring to Fig. 4a once again, among the HT-ausformed steels A, C and D at the same hardness level of about 440 HV10, the HT-ausformed steel A showed the least abrasive wear resistance, which could be correlated to its microstructure: the BFF was largest for the HT-A. Also, the LT-B and LT-C at the same hardness level showed lower mass loss for the sample with lower BFF. However, the comparison of BFF was very difficult between the steels due to the different features included in the calculations. Hence, the BFF size cannot be clearly stated to have a direct effect on the work-hardening or wear resistance, but it should be considered as one important feature affecting the work-hardening and subsequently wear resistance.

As a result, the CFB steels with the capability to undergo extensive work-hardening and inherent lower susceptibility to white layer and shear band formation provide a promising combination for possible wear-resistant steels. In the current work, some CFB variants outperformed the martensitic steel irrespective of the initial hardness. Moreover, the possibility to produce CFB steels with even higher hardness could provide even further enhanced wear performance matching or exceeding high-hardness (> 600 HB) martensitic steels. For future considerations, the wear testing of CFB steels should be continued with other wear testing devices and higher sample count for more comprehensive knowledge on the wear resistance. Furthermore, the microstructural features should be determined more carefully for better understanding on the factors affecting the wear performance.

5. Summary and conclusions

Several carbide-free bainitic steels were produced via three different ausforming methods. The steels were tested for mechanical properties and abrasive wear resistance. Microstructural features were characterized from both unworn and worn samples. The following conclusions were made:

(1) The produced microstructures consisted of different fractions of bainitic ferrite or granular bainite (56–68%), martensite (0–25%) and retained austenite (20–34%), which was discovered as coarse pools and inter-lath films in the microstructure. The high-temperature ausforming at 850 °C resulted in most martensite fraction, while the low-temperature ausforming (450 °C) produced the highest retained austenite content and least martensite. The medium-temperature (550 °C) ausforming lead varying fractions of the phases due to the difficulty in controlling the temperature.

(2) The experimental carbide-free bainitic steels produced via three different ausforming routes exhibited high mechanical properties with yield strength between 700-900 MPa and tensile strength in the range of 1300–1900 MPa. Yield ratio was generally low (0.43–0.64) and total elongation was varying from 7.9 to 25.2%. The highest hardness (535 ± 22 HV10) and tensile strength (1912 ± 9 MPa) were measured for the medium-temperature ausformed steel with the highest carbon content. Steel samples ausformed at low temperature (450 °C) had higher elongation and decresed hardness, while the medium-temperature ausformed steels showed the highest strength. The high-temperature forming (850 °C) resulted in mechanical properties averaging between the two other ausforming treatments.

(3) High-stress abrasive wear testing in the form of dry-pot pin-mill tester was utilized for measuring the wear performance reported as mass loss. The lowest mass loss was measured for the MT-E sample, which also had the highest initial hardness, while the same hardness level commercial martensitic 500HB grade steel exhibited higher mass loss. The hardness-to-mass loss ratio was found very promising with some of the experimental carbide-free bainitic steels outperforming the reference martensitic steel.

(4) The high work-hardening capability of the carbide-free bainitic steels was the main factor resulting in the superior abrasive wear resistance. The mixture of bainite, martensite, and retained austenite resulted in the surface with sufficient initial hardness

while maintaining the capability for extensive hardening due to the strain-induced transformation of austenite to martensite.

Declaration of competing interest

The authors declare that they have no known competing financial interests or personal relationships that could have appeared to influence the work reported in this paper.

CRediT authorship contribution statement

Oskari Haiko: Writing - original draft, Formal analysis, Investigation, Resources, Visualization, Data curation, Conceptualization. **Pentti Kaikkonen:** Writing - original draft, Formal analysis, Investigation, Resources, Visualization. **Mahesh Somani:** Writing - review & editing, Conceptualization, Supervision. **Kati Valtonen:** Writing - review & editing. **Jukka Kömi:** Project administration, Supervision.

Acknowledgements

This study has received support from RFCS under contract RFCS-2015-709607 TIANOBAIN, and project partners are also acknowledged for providing materials.

Appendix A. Supplementary data

Supplementary data to this article can be found online at https://doi.org/10.1016/j.wear.2020.203386.

References

[1] O. Haiko, M. Somani, D. Porter, P. Kantanen, J. Kömi, N. Ojala, et al., Comparison of impact-abrasive wear characteristics and performance of direct quenched (DQ) and direct quenched and partitioned (DQ&P) steels, Wear 400–401 (2018) 21–30, https://doi.org/10.1016/j.wear.2017.12.016.

[2] S.G. Liu, S.S. Dong, F. Yang, L. Li, B. Hu, F.H. Xiao, et al., Application of quenching-partitioning-tempering process and modification to a newly designed ultrahigh carbon steel, Mater. Des. 56 (2014) 37–43, https://doi.org/10.1016/j.matdes.2013.10.094.

[3] E. Vuorinen, N. Ojala, V. Heino, C. Rau, C. Gahm, Erosive and abrasive wear performance of carbide free bainitic steels - comparison of field and laboratory experiments, Tribol. Int. 98 (2016) 108–115, https://doi.org/10.1016/j.triboint.2016.02.015.

[4] B. Prakash, F.G. Caballero, R. Elvira, V. Smanio, T. Sourmail, C. Garcia-Mateo, et al., Wear of nano-structured carbide-free bainitic steels under dry rolling–sliding conditions, Wear 298–299 (2012) 42–47, https://doi.org/10.1016/j.wear.2012.11.064.

[5] W. Wang, R. Song, S. Peng, Z. Pei, Multiphase steel with improved impact-abrasive wear resistance in comparison with conventional Hadfield steel, Mater. Des. 105 (2016) 96–105, https://doi.org/10.1016/j.matdes.2016.05.056.

[6] X. Xu, W. Xu, F.H. Ederveen, S. van der Zwaag, Design of low hardness abrasion resistant steels, Wear 301 (2013) 89–93, https://doi.org/10.1016/j.wear.2013.01.002.

[7] B. Avishan, S. Yazdani, S. Hossein Nedjad, Toughness variations in nanostructured bainitic steels, Mater. Sci. Eng. 548 (2012) 106–111, https://doi.org/10.1016/j.msea.2012.03.098.

[8] V.G. Efremenko, O. Hesse, T. Friedrich, M. Kunert, M.N. Brykov, K. Shimizu, et al., Two-body abrasion resistance of high-carbon high-silicon steel: metastable austenite vs nanostructured bainite, Wear 419 (2019) 24–35, https://doi.org/10.1016/j.wear.2018.11.003.

[9] C. Garcia-Mateo, F.G. Caballero, T. Sourmail, M. Kuntz, J. Cornide, V. Smanio, et al., Tensile behaviour of a nanocrystalline bainitic steel containing 3wt% silicon, Mater. Sci. Eng. 549 (2012) 185–192, https://doi.org/10.1016/j.msea.2012.04.031.

[10] T. Sourmail, F.G. Caballero, C. Garcia-Mateo, V. Smanio, C. Ziegler, M. Kuntz, et al., Evaluation of potential of high Si high C steel nanostructured bainite for wear and fatigue applications, Mater. Sci. Technol. 29 (2013) 1166–1173, https://doi.org/10.1179/1743284713Y.0000000242.

[11] H.K.D.H. Bhadeshia, D.V. Edmonds, Bainite in steels: new composition-property approach Part 1, Met. Sci. 17 (1983) 411–419.

[12] A. Sundström, J. Rendón, M. Olsson, Wear behaviour of some low alloyed steels under combined impact/abrasion contact conditions, Wear 250 (2001) 744–754, https://doi.org/10.1016/S0043-1648(01)00712-8.

[13] J. Rendón, M. Olsson, Abrasive Wear Resistance of Some Commercial Abrasion Resistant Steels Evaluated by Laboratory Test Methods, vol. 267, 2009, pp. 2055–2061, https://doi.org/10.1016/j.wear.2009.08.005.

[14] B. Narayanaswamy, P. Hodgson, H. Beladi, Comparisons of the two-body abrasive wear behaviour of four different ferrous microstructures with similar hardness levels, Wear 350–351 (2016) 155–165, https://doi.org/10.1016/j.wear.2016.01.013.

[15] M. Shah, S. Das Bakshi, Three-body abrasive wear of carbide-free bainite, martensite and bainite-martensite structure of similar hardness, Wear 402–403 (2018) 207–215, https://doi.org/10.1016/j.wear.2018.02.020.

[16] E. Vuorinen, V. Heino, N. Ojala, O. Haiko, A. Hedayati, Erosive-abrasive wear behavior of carbide-free bainitic and boron steels compared in simulated field conditions, Proc. Inst. Mech. Eng. Part J J. Eng. Tribol. 232 (2018) 3–13, https://doi.org/10.1177/1350650117739125.

[17] B. Liu, W. Li, X. Lu, X. Jia, X. Jin, The effect of retained austenite stability on impact-abrasion wear resistance in carbide-free bainitic steels, Wear 428–429 (2019) 127–136, https://doi.org/10.1016/j.wear.2019.02.032.

[18] A.M. Gola, M. Ghadamgahi, S.W. Ooi, Microstructure evolution of carbide-free bainitic steels under abrasive wear conditions, Wear 376–377 (2017) 975–982, https://doi.org/10.1016/j.wear.2016.12.038.

[19] P.M. Kaikkonen, M.C. Somani, I.H. Miettunen, D.A. Porter, Constitutive flow behaviour of austenite at low temperatures and its influence on bainite transformation characteristics of ausformed, Mater. Sci. Eng., A 775 (2020) 9–11, https://doi.org/10.1016/j.msea.2020.138980.

[20] ASTM E562-01, Standard Test Method for Determining Volume Fraction by Systematic Manual Point Count, 2000.

[21] K. Valtonen, N. Ojala, O. Haiko, V. Kuokkala, Comparison of various high-stress wear conditions and wear performance of martensitic steels, Wear 426–427 (2019) 3–13, https://doi.org/10.1016/j.wear.2018.12.006.

[22] K. Valtonen, K. Keltamäki, V.T. Kuokkala, High-stress abrasion of wear resistant steels in the cutting edges of loader buckets, Tribol. Int. 119 (2018) 707–720, https://doi.org/10.1016/j.triboint.2017.12.013.

[23] K. Valtonen, V. Ratia, N. Ojala, V.-T. Kuokkala, Comparison of laboratory wear test results with the in-service performance of cutting edges of loader buckets, Wear 388–389 (2017) 93–100, https://doi.org/10.1016/j.wear.2017.06.005.

[24] O. Haiko, K. Valtonen, A. Kaijalainen, S. Uusikallio, J. Hannula, T. Liimatainen, et al., Effect of tempering on the impact-abrasive and abrasive wear resistance of ultra-high strength steels, Wear (2019) 440–441, https://doi.org/10.1016/j.wear.2019.203098.

[25] ISO 4287:1997 Geometrical Product Specifications (GPS) — Surface Texture: Profile Method — Terms, Definitions and Surface Texture Parameters, 1997.

[26] M.N. Yoozbashi, S. Yazdani, XRD and TEM study of bainitic ferrite plate thickness in nanostructured, carbide free bainitic steels, Mater. Chem. Phys. 160 (2015) 148–154, https://doi.org/10.1016/j.matchemphys.2015.03.071.

[27] C. Garcia-Mateo, J.A. Jimenez, B. Lopez-Ezquerra, R. Rementeria, L. Morales-Rivas, M. Kuntz, et al., Analyzing the scale of the bainitic ferrite plates by XRD, SEM and TEM, Mater. Char. 122 (2016) 83–89, https://doi.org/10.1016/j.matchar.2016.10.023.

[28] Y.B. Xu, Y.L. Bai, Q. Xue, L.T. Shen, Formation, microstructure and development of the localized shear deformation in low-carbon steels, Acta Mater. 44 (1996) 1917–1926, https://doi.org/10.1016/1359-6454(95)00306-1.

[29] E. Broitman, Indentation hardness measurements at macro-, micro-, and nanoscale: a critical overview, Tribol. Lett. 65 (2017) 1–18, https://doi.org/10.1007/s11249-016-0805-5.

[30] A. Sundström, J. Rendon, M. Olsson, Wear behaviour of some low alloyed steels under combined impact/abrasion contact conditions, Wear 250 (2001) 744–754, https://doi.org/10.1016/S0043-1648(01)00712-8.